American Journal of Aerospace Engineering
2016; 3(2): 13-23
http://www.sciencepublishinggroup.com/j/ajae
doi: 10.11648/j.ajae.20160302.12
ISSN: 2376-4813 (Print); ISSN: 2376-4821 (Online)

Methodology Article

Determination of Required Torque to Spin Aircraft Wheel at Approach Using ANSYS CFX

Abdurrhman A. Alroqi, Weiji Wang

Department of Engineering and Design, University of Sussex, Brighton, UK

Email address:
aa-alroqi@hotmail.com (A. A. Alroqi), W.J.Wang@sussex.ac.uk (Weiji Wang)

To cite this article:
Abdurrhman A. Alroqi, Weiji Wang. Determination of Required Torque to Spin Aircraft Wheel at Approach Using ANSYS CFX. *American Journal of Aerospace Engineering*. Vol. 3, No. 2, 2016, pp. 13-23. doi: 10.11648/j.ajae.20160302.12

Received: April 9, 2016; **Accepted**: April 20, 2016; **Published**: May 3, 2016

Abstract: Many patents have suggested that spinning the aircraft wheel before touchdown would lessen tyre wear as indicated by landing smoke and rubber deposites on the runway caused by skidding wheel at the point of impact. In this paper, the required torque to spin the aircraft wheel at approach speed has been calculated using ANSYS Workbench CFX, which is used to determine the wheel aerodynamic forces developed by simulation of fluid flows in a virtual environment. The wheel has been tested against different wind speeds, and the aerodynamic forces for the spinning wheel are presented, which include; translational and rotational drags, lift created by vortex, and shaft rolling resistance.

Keywords: Spinning Aircraft Wheel, Aerodynamic Force, Translational Drag, Rotational Drag, SST Turbulence RANS Model, ANSYS CFX

1. Introduction

Spinning the aircraft wheel before touchdown is a proposed solution to eliminate the smoke generated between the tyres and runway at landing impact [1-9]. The landing smoke phenomenon is described by the following chain events: firstly, the aircraft approaches the runway at a relatively high speed. Therefore, a high velocity difference exists between the wheels and runway, which leads to the tyres being fully locked on the runway at landing until the friction force at the contact surface increases sufficiently for the wheel to 'spin-up' and to reach a constant angular velocity which is equivalent to aircrafts forward speed [10].

During the skidding phase, a high temperature is generated in the tyre tread rubber, sufficient in fact to locally melt the rubber. The melted rubber becomes weak enough for tyre wear to take place [11]. Part of worn rubber sticks to the runway whilst the remaining part is burnt-off forming the distinctive puff of white smoke [12].

In this paper, a case study of Boeing 747-400 main landing wheel has been modelled using ANSYS CFX in order to calculate the required torque to spin the wheel in the aircraft approach phase.

The wheel is tested against three high wind speeds. The lowest wind speed is at least equal to aircraft approach speed in order to simulate the case of a zero heading wind. The model represents the forces created during wheel rotation. Finally, the torque necessary to spin the wheel for required rotation is presented.

1.1. Literature Review

Kothawala, Gatto and Wrobel carried out a computational investigation of the combined effect of Yaw, rotation and Ground proximity on aerodynamics of an isolated wheel using steady and unsteady Reynolds-Averaged Navier-Stokes (RANS & URANS). The diameter and width of the wheel was 0.416m and 0.191m respectively. They tested the rotated wheel against a free stream of air with speeds of 70 and 98 m/s. The wheel rotation speeds were 100, 200, and 327 rad/sec. However, they conclude that the wake on rear of wheel increases with increased rotation speeds [13].

Morelli tested a stationary and rotated wheel against the same wind speed using a wind tunnel. He found that the drag is increases by about 10% when the wheel is rotating. He concluded that this increase of drag was due to negative lift and induced drag [14].

Rahman carried out a computational study on flow around a rotating short cylinder in order to study the effect of rotation on the aerodynamics forces. The cylinder considered is in X-Y plane, the rotation is about the Z axis, and the flow is along the positive x - direction. He found that the clockwise rotation of the cylinder reduced the pressure region above the cylinder with higher pressure at the bottom surface. The difference in pressure producing an upward lift force for clockwise rotation and vice versa for anticlockwise. Also, the lift force is dependent on the cylinder spin ratio, an increase in the rotational velocity producing an increasing lift force [15].

1.2. Case Study Data

The wind speeds used in this simulation are; 80.7, 100, and 120 m/s. The first wind speed (80.7 m/s) is equal to the Boeing 747-400 approach speed whilst the other higher speeds are assumed in case of heading wind speed increase [16]. The wheel geometry data is presented in Table 1 [17, 18].

For required wheel rotation speed, it is important to know the aircraft touchdown speed in order to calculate the equivalent wheel rotation speed with regard to tyre deflection. However, the aircraft will lose about 10 knots (5.14 m/s) during the flare manoeuvre before touchdown, which results in a 75.6 m/s forward speed [19].

The tyre deflects upon landing impact, which means a lesser radius during rotation.

For simplification, the tyre free rolling velocity is assumed to be 121 rad/sec, this is calculated using the tyre radius and aircraft forward speed on the runway. Here we will simulate 50% of the wheel full free rotation, this is because the aircraft wheel is heavy and consequently it may requires large wind turbines for full spinning. Moreover, designing the turbine for full wheel rotation may lead to excessive free rolling rotation, e.g. in the case of high head wind speed, while using the 50% of free rotation with wind speed equivalent to the aircraft approach speed to design the turbine will guarantee it rotates at the minimum wind speed. This gives the turbine the opportunity to rotate in a safe mode if the head wind were to increase.

Table 1. *Wheel geometry data.*

	Weight (kg)	Radius (mm)	Width (mm)
Tyre	110	622.3	482.6
Rim	74.4	255	-------

2. Theoretical Background

In this model, it is assumed that the wheel is moving through the air with zero angle of attack and the direction of rotation of the wheel is anticlockwise. The wheel will accelerate from zero to the required rotational speed. Fig. 1 shows the forces to be calculated in order to determine the torque is required to spin the wheel. The wind turbine should be physically attached to the wheel rim to consider the tyre deflection effect at touchdown. In this case, the rim mean radius is the force arm to calculate the required torque to be as:

$$T_{required} = F_{required}\, r_{rim} \tag{1}$$

where, $T_{required}$ and $F_{required}$ are the required torque (N.m) and the required force (N) to spin the wheel respectively, and r_{rim} is the mean radius of the rim (m), which depends on the wind turbine position.

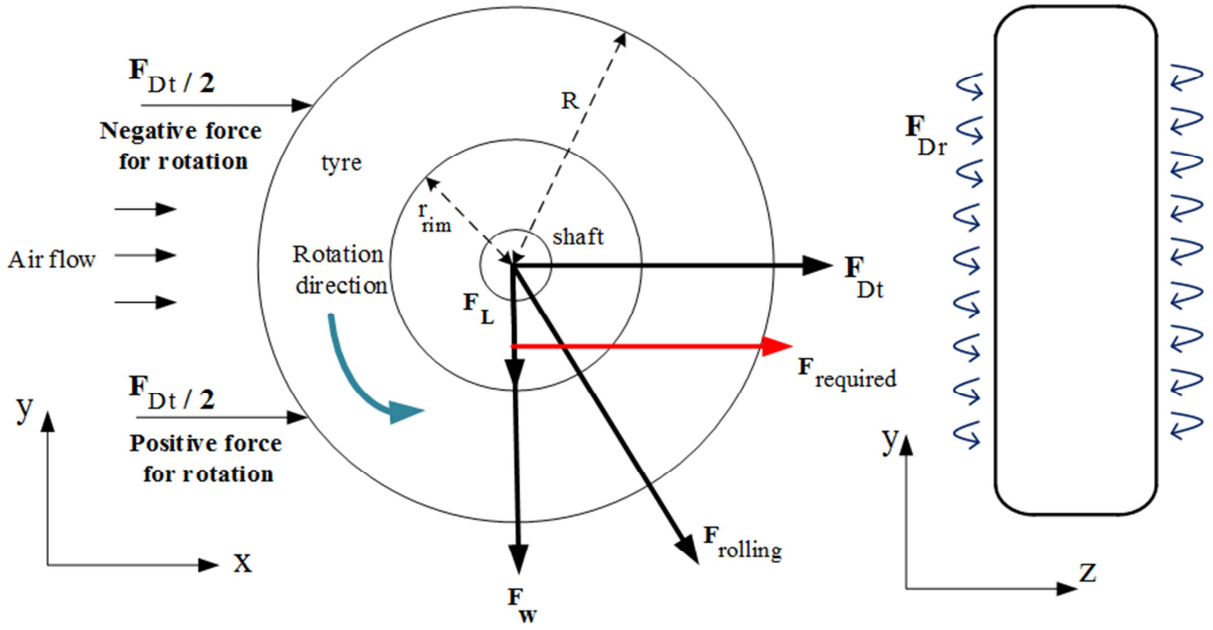

Fig. 1. *External forces acting on the rotating wheel.*

The required force should be at least equal to the sum of all wheel forces including to the aerodynamic forces some of which will be generated during the wheel rotation. Therefore, the required force will be as:

$$F_{required} = F_{ei} + F_D + F_{rolling} \tag{2}$$

where, F_{ei} is the equivalent inertial force during acceleration (N), F_D is the total drag force, which is inclusive of the translational and rotational drags (N), and $F_{rolling}$ is the shaft rolling resistance (N).

2.1. Drag Force

There are two types of drag force. Firstly, the translational drag in x direction (F_{Dt}), which impacts the wheel frontal area as shown in Fig. 1. Half of this force is positive for rotation and other half is negative "resistance" and because the wheel is symmetrical, therefore, the two parts have an equal and opposite effect in the static condition and the resultant torque on the wheel shaft becomes zero.

On the other hand, the total force, will be applied to the wheel shaft in x direction which will increase the rolling resistance.

The formula of translational drag can be calculated as:

$$F_{Dt} = \frac{1}{2}\,\rho\, C_{Dt}\, A_f\, U^2 \tag{3}$$

where, ρ is the air density (kg/m^3), C_{Dt} is the translational drag coefficient, U is the wind speed acts on the wheel (m/sec), and A_f is the wheel frontal area (m^2) [20]. The frontal area is roughly half the wheel circumference area; $A_f = R\pi D$, here R and D are wheel radius and width respectively. The force on the wheel frontal area is different from centre to the top or bottom surfaces.

Once the wheel starts to rotate, half of this force in the positive direction becomes higher than the one in negative direction which is effected by the wheel rotation direction, this force is helpful as it will be added to the required force for spinning the wheel.

The other drag force is that created during wheel rotation and it is called "rotational drag force" which increases in magnitude with increasing wheel angular velocity and occurs around the two side areas of the wheel, acting in the rotation (z) axis. The rotational drag can be calculated by this formula:

$$F_{Dr} = \frac{1}{2}\,\rho\, C_{Dr}\, A_{side}\, R^2\omega^2 \tag{4}$$

where, C_{Dr} is the rotational drag coefficient, A_{side} is the two side areas of the wheel (m^2), R is the wheel radius (m), and ω is the wheel angular velocity (rad/sec) [21].

2.2. Rolling Resistance Force

Three types of force act on the wheel shaft in x and y directions resulting in the total magnitude force, $F_{rolling}$. The three forces are, as follows:

1. Translation drag force (F_{Dt}) presented in (3), is applied to the shaft in (x) direction.
2. The wheel weight force, F_w in ($-y$) and is simply; $F_w = mg$, where, m is the wheel total mass, and g is the acceleration due to gravity.
3. The lift force, which is created during the wheel rotation.

Kutta-Joukowski lift theorem for a cylinder describes how this force depends on the direction of rotation and acts perpendicular to the air flow direction. As shown in Fig. 2, the wheel is pulling a thin layer of flow molecules in its rotation direction resulting in a faster flow on the lower surface than on the upper surface, which leads to less pressure than wheel top surface. The wheel upper surface will also pull a thin layer in the opposite direction to the flow which creates a vortex. This vortex has the effect of increasing the upper pressure. The difference in pressure between the wheel top and bottom surfaces is the lift force. In our case, the negative (downward) lift force increases the resistance on the shaft because it acts in same direction as the wheel weight force.

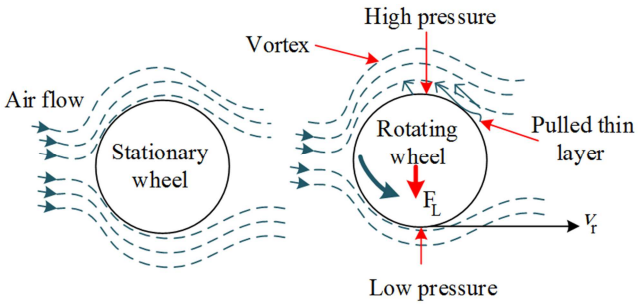

Fig. 2. *Lift force created during wheel rotation.*

The lift force can be calculated as:

$$F_L = \rho\, G\, U \tag{5}$$

where, G is the vortex strength (m^2/sec) and is given by [22]:

$$G = 2\,\pi\, R\, v_r \tag{6}$$

where, v_r is the relative wheel speed (rad/sec), and it is given by: $v_r = R\omega$. The relative speed gives the spin ratio as: $\frac{v_r}{U}$. The increasing of the spin ratio causes an increasing in the lift force [15, 23, 24].

Substituting (6) in (5) with respect to the wheel angular velocity, the lift force will be as:

$$F_L = 2\,\rho\,\pi\, R^2\,\omega \tag{7}$$

Because all the parameters in (7) are unchanged with the exception of the wheel angular velocity, therefore, the lift force is zero with a stationary wheel, and increases with increasing wheel rotation speed.

Now, simply the total force acting on the wheel shaft will be as:

$$F_{ts} = \sqrt{(F_w + F_L)^2 + {F_{Dt}}^2} \tag{8}$$

where, F_{ts} is the total force applied to the shaft. Note: The term $(F_w + F_L)$ will be $(F_w - F_L)$ if the wheel rotate clockwise with the same current flow direction.

The bearing friction coefficient must be considered to estimate the rolling resistance. Therefore, the shaft rolling resistance force will be as [25]:

$$F_{rolling} = C_r\, F_{ts} \tag{9}$$

where, C_r is the bearing friction coefficient, assumed to be angular contact ball bearing with value of 0.0015 [26].

2.3. Equivalent Inertial Force During Acceleration

This force is internal which is the resistance of the wheel against its acceleration. Using Newton's second law, this force can be expressed as:

$$F_{ei} = m\,\dot{\omega} \tag{10}$$

where, $\dot{\omega}$ is the wheel angular acceleration (rad/s^2), and can be calculated as:

$$\dot{\omega} = \frac{d\omega}{dt} \tag{11}$$

where, t is the acceleration time (sec). Rewriting (10) with respect to (11), to be:

$$F_{ei} = m\,\frac{d\omega}{dt} \tag{12}$$

From (12), this force depends on the time required to complete the acceleration and it decrease to about zero at $(t = \infty)$.

Slow acceleration requires less force and Vice versa. However, the wheel aerodynamics forces is fall into the category of experimental science [27]. Therefore, the wheel is modelled using ANSYS CFX to calculate both the forces and the required torque. The wheel is rotated from zero to 60.5 rad/sec during first four seconds with constant acceleration maintaining a constant angular speed for a further two seconds.

The purpose of spinning the wheel is to investigate the wheel aerodynamic forces generated during rotation, these forces are not present on a stationary wheel.

3. Simulation Model

The present work describes a thorough investigation of 3D computations concerning the air flow around the wheel. The calculated results give a clear indication of the air flow distributions for different inlet velocity values. Modelling tasks using CFD programs will allow us to get closer to the real operating conditions.

The 3D wheel geometry is modelled using the ANSYS design modeller together with the data as presented in Table 1. The wheel modelled inside the large domain is as shown in Fig. 3.; the tyre being soft without grooves. The domain dimensions are 20 m x 20 m inlet area by 40 m long to avoid the wall boundary effect and so be representative of the real aircraft wheel conditions during approach in open air.

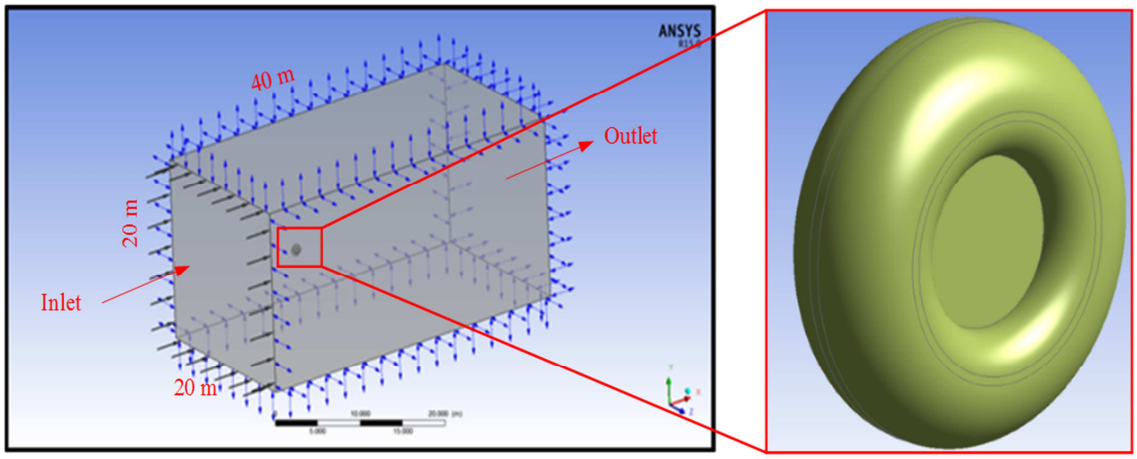

Fig. 3. *Wheel domain.*

3.1. Mesh Generating

High-quality mesh created for accurate solutions and good convergence. A "Patch Conforming Method" is used to generate the mesh with tetrahedron form elements. In addition, prismatic layers are constructed for the flow near the walls and on the wheel surfaces using "smooth transition" option for more accuracy [28].

The flow regime is subsonic with static temperature at 288 K and the turbulence is zero gradient. Reference and relative Pressures are 1 and $1.013x10^5$ pa. Rough wall surfaces are used as the SST model does not accurately predict the amount and onset of the flow separation from soft surfaces [29]. Fig. 4 shows the mesh model, and Table 2 presents the mesh statistics. The boundary conditions are the same for all simulations except the inlet velocities.

Table 2. *Mesh statistics.*

	Value
nodes	9197
elements	43703
tetrahedrons	39663
prisms	4040
faces	1952
Orthogonality Angle [30]	27.4^0, acceptable range $> 20^0$
Expansion factor	20^0, acceptable range $< 20^0$
Aspect Ratio	57^0, acceptable range $< 100^0$

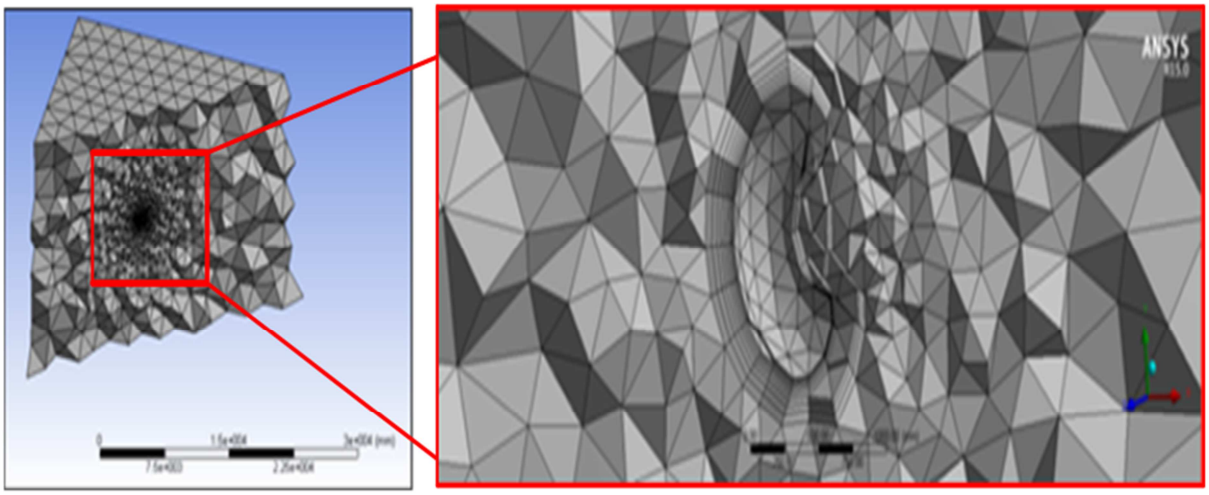

Fig. 4. *Mesh model of the Wheel domain.*

The flow type and the physical model in the fluid domain is defined as 'steady state' with turbulence conditions using Reynolds-Averaged Navier-Stokes equations. Turbulence is modelled using the SST (Shear Stress Transport) model and heat transfer using the total energy model.

The SST turbulence model is commonly used and is suitable for a wide range of applications.

The total energy model allows for high speed energy effects and is therefore, suitable for high speed flow applications and has better performance at wall boundaries [31, 32].

3.2. SST Turbulence RANS Model

The RANS model allows us to simulate turbulent flow as a steady state. Fig. 5 shows a simple definition for flow velocities in the RANS model.

The flow velocity is calculated as:

$$U(\vec{x},t) = \bar{U}(\vec{x}) + u'(\vec{x})$$

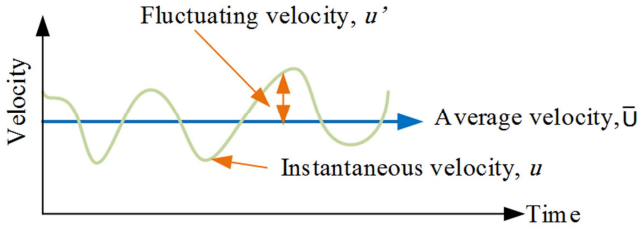

Fig. 5. *Velocities definition in RANS model.*

Applying the time average procedure to the governing equation which gives the Reynolds-Averaged Navier-Stokes (RANS) equations to be as:

$$\frac{\partial(\rho\overline{u_i})}{\partial t} + \frac{\partial(\overline{u_i}\,\overline{u_j})}{\partial x_j}$$

$$= -\frac{\partial \bar{P}}{\partial x_i} + \frac{\partial}{\partial x_j}\left[\mu\left(\frac{\partial \overline{u_i}}{\partial x_j} + \frac{\partial \overline{u_j}}{\partial x_i} - \frac{2}{3}\delta_{ij}\frac{\partial \overline{u_m}}{\partial x_m}\right)\right] + \frac{\partial}{\partial x_j}\left(-\rho\,\overline{u_i'u_j'}\right)$$

here, $-\rho\,\overline{u_i'u_j'} = R_{ij}$ which is Reynolds stress tensor.

SST model:

$$\frac{\partial(\rho k)}{\partial t} + \frac{\partial(\rho U_i k)}{\partial x_i} = \bar{P}_k - \beta^*\rho k\omega + \frac{\partial}{\partial x_i}\left[(\mu + \rho_k\mu_t)\frac{\partial k}{\partial x_i}\right]$$

$$\frac{\partial(\rho\omega)}{\partial t} + \frac{\partial(\rho U_i\omega)}{\partial x_i} = \alpha\frac{1}{v_t}\tilde{P}_k - \beta\rho\omega^2 + \frac{\partial}{\partial x_i}\left[(\mu + \sigma_\omega\mu_t)\frac{\partial\omega}{\partial x_i}\right] + 2(1-F_1)\rho\sigma_{\omega 2}\frac{1}{\omega}\frac{\partial k}{\partial x_i}\frac{\partial\omega}{\partial x_i}$$

$$v_t = \frac{a_1 k}{\max(a_1\omega, SF_2)};\ S = \sqrt{2S_{ij}\,S_{ij}}$$

$$P_k = \mu_t\frac{\partial U_i}{\partial x_j}\left(\frac{\partial U_i}{\partial x_j} + \frac{\partial U_j}{\partial x_j}\right),$$

$$\tilde{P}_k = \min(P_k, 10.\beta^*\rho k\omega),$$

$$\mu_t = \rho\frac{k}{\omega},$$

$$F_1 = tanh\left\{\left\{\min\left[max\left(\frac{\sqrt{k}}{\beta^*\omega Y}, \frac{500v}{Y^2\omega}\right), \frac{4\rho\sigma_{\omega 2}k}{CD_{k\omega}Y^2}\right\}^4\right\},$$

$$F_2 = \tanh\left[\left[\max\left(\frac{2\sqrt{k}}{\beta^* wY}, \frac{500v}{Y^2\omega}\right)\right]^2\right],$$

$$CD_{k\omega} = \max\left(2\rho\sigma_{\omega 2}\frac{1\partial k\partial\omega}{\omega\partial x_i\partial x_i}, 10^{-10}\right)$$

where, k and ω are the turbulence kinetic energy and frequency respectively, Y is the distance to the wall boundary, S is the mean strain tensor rate, $F_{1,2}$ are blending function, which is equal to one. The constants are defined as: $\alpha = \alpha_1 F_1 + \alpha_2(1-F_1)\ldots$ etc., $\beta^* = 0.09$, $\alpha_1 = 5/9$, $\beta_1 = 3/4$, $\sigma_{k1} = 0.85, \sigma_{\omega 1} = 0.5$, $\alpha_2 = 0.44$, $\beta_2 = 0.0828$, $\sigma_{k2} = 1$, $\sigma_{\omega 2} = 0.856$ [29, 31].

4. Results and Discussion

A comparison of the air flow around the wheel at three wind speeds; 80.7, 100, and 120 m/s is shown in Fig. 6. As shown in velocity x-y diagrams, a thin layer of flow molecules is pulled

by the wheel in the rotation direction. At the top of the wheel, the layer of flow is in the opposite direction to that of the wind which created the vortex, this has the effect of increasing the pressure at the top of the wheel, thus producing a negative lift force. Moreover, the wind speed is higher at the wheel bottom with consequently less pressure than the top wheel area, which leads to the total overall vertical force acting on the wheel to be in a downward direction. The lift force varies directly as the wind speed, that is the higher the wind speed the higher the lift force developed. The air flow speed behind the wheel is approximately zero for all wind speeds, which is in agreement with [13].

In general, an increase in the wind speed produces a corresponding increase in the aerodynamic forces around the wheel.

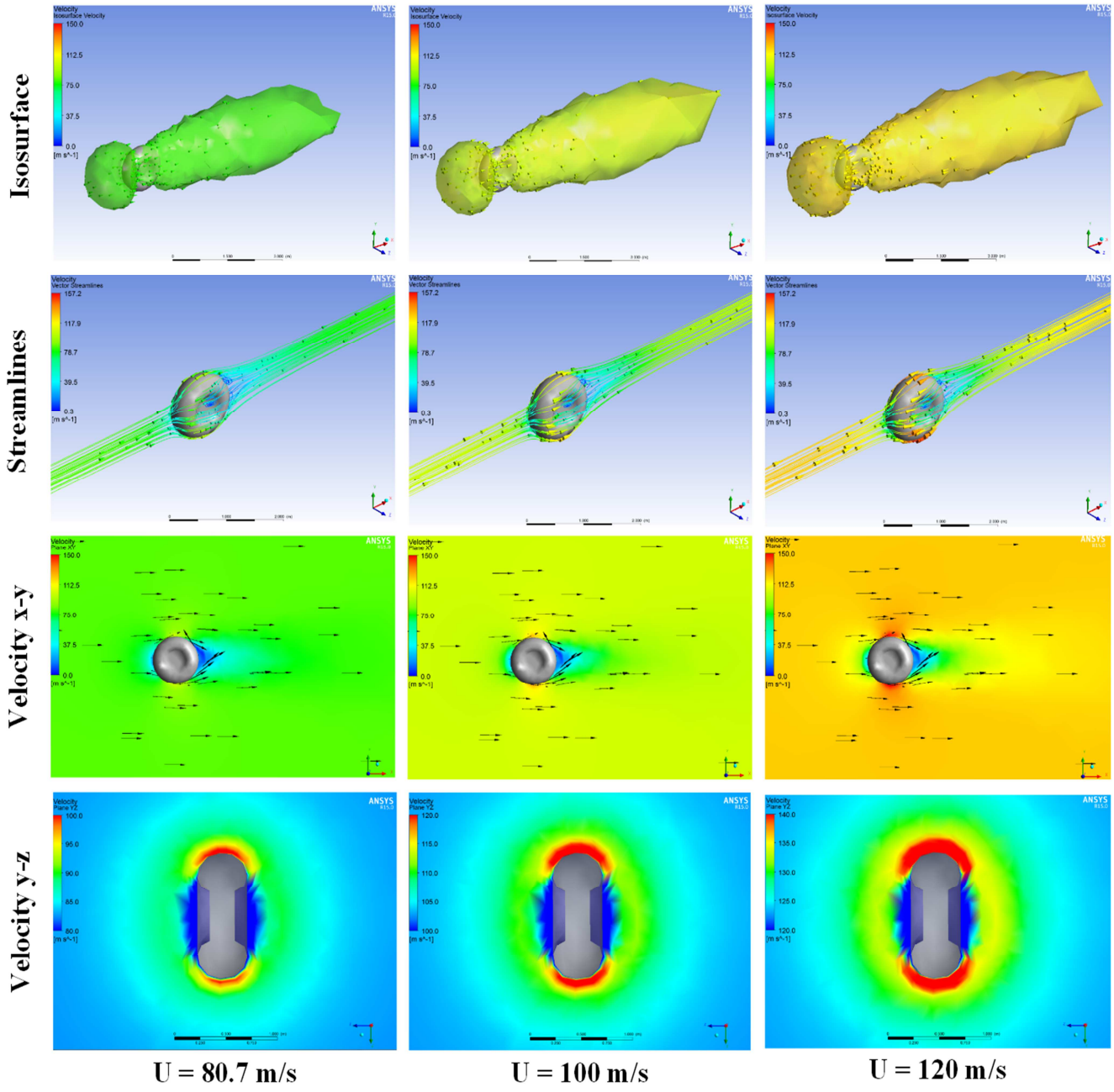

Fig. 6. A comparison of different flow profiles around the wheel at different wind speeds.

4.1. Translational Drag Force

The impact of wind flow on the wheel shows different characteristic force behaviour, which is speed dependant. The translational drag force at high wind speeds (100 and 120 m/s) increases over its steady state value immediately to settled down shortly afterwards. This impact force has the effect of increasing the resistance on the wheel shaft. The translational drag force at the three different wind speeds all show steady values after a period of one second, even while the wheel accelerates. A Comparison of the force curves and distribution profiles are presented in Fig. 7 and Fig. 8 respectively.

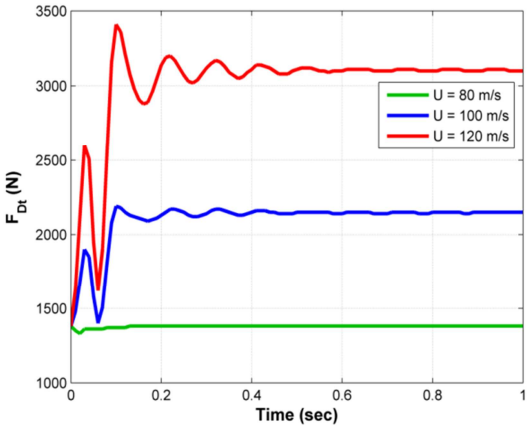

Fig. 7. *A comparison of translation drag forces vs. time with different wind speeds.*

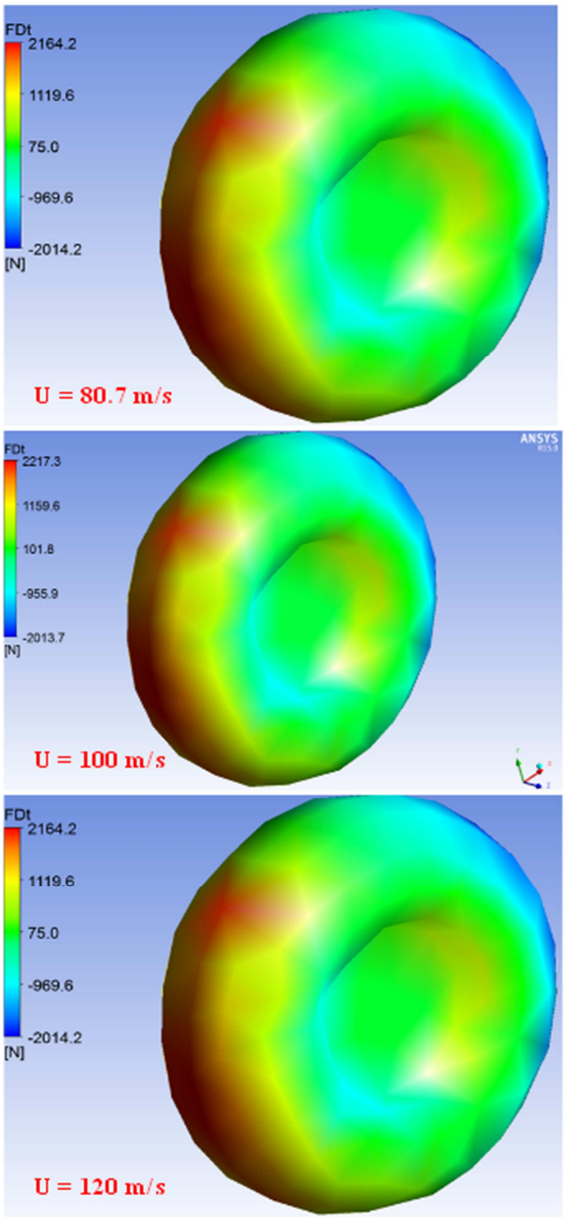

Fig. 8. *Contours of translational drag force with different wind speeds.*

At a wind speed of 80.7 m/s, a drag force of 1383 N is generated by the air flow, which impinges the wheel frontal area at the moment of impact.

Once the wheel starts to rotate, it is seen that the force drops to 1331 N only to increase to 1370 N within 0.09 sec before reaching a steady state value of 1380 N, which is close to the value of a stationary wheel.

At a wind speed of 100 m/s, the force increases immediately from 1383 N to 1900 N within 0.03 seconds. After a further 0.06 seconds it has decreased to 1400 N only to recover and increase again, reaching a steady state value of 2150 N within 0.89 seconds following some slight undulations.

At a wind speed of 120 m/s, the force behaviour is similar to that generated by the 100 m/s wind speed except with higher values. The peak value being 3410 N within 0.1 seconds which settled down to steady state value of 3100 N after 0.97 seconds.

4.2. Side Force - Including Rotational Drag

The rotational and side drag force increases from 64.8 N during wheel acceleration to reach a steady state at ultimate wheel rotation velocity. The resultant rotational drag force acts in the (-z) direction that because the flow acts on the rim side to push the wheel as it larger side area than the other part.

According to rotational drag force formula, it is created during wheel rotation, but as the wheel aerodynamic force is determined by experimental science, this simulation shows that the flow is producing drag force on the wheel sides area because of the tyre shape which is include breadth.

Moreover, the flow is pulled inside the hub and then re-circulated. This re-circulated flow impinges on the free air flow straight past the wheel. Therefore, the force of rotational drag here is inclusive of translation drag on the wheel sides, which is affected by wind speeds. However, Fig. 9 and Fig. 10 shows force curves generated during wheel acceleration and a comparison of wheel profiles at different wind speeds respectively. For all wind speeds, the force starts with the same value of 64.8 N.

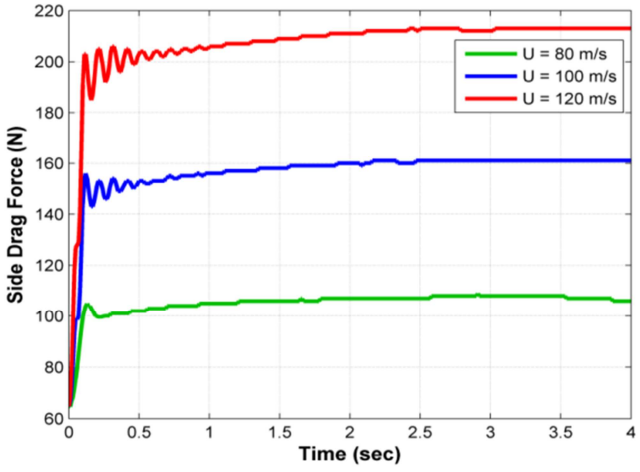

Fig. 9. *A comparison of side drag forces vs. time with different wind speeds.*

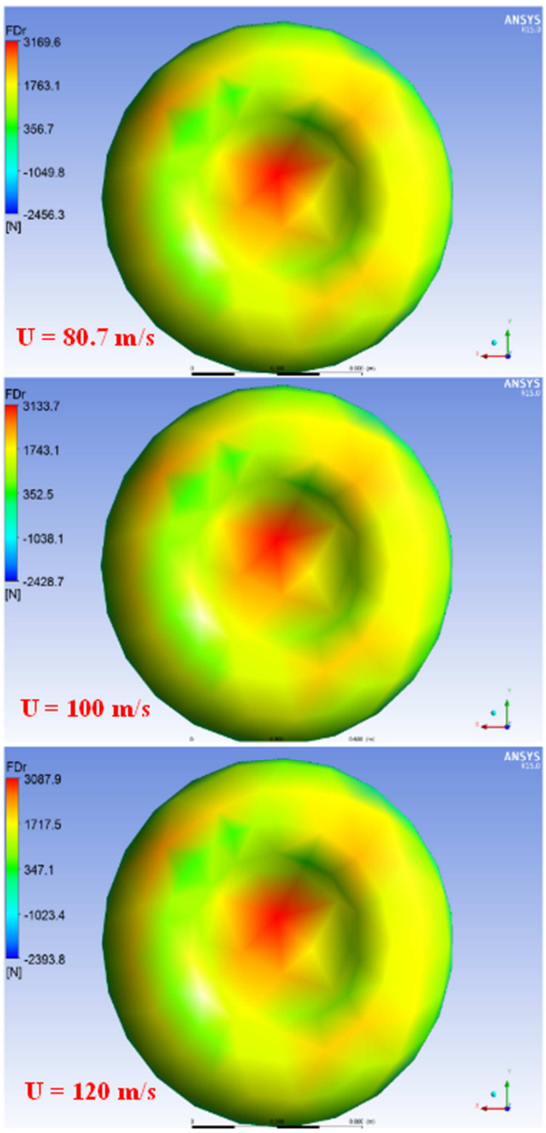

Fig. 10. *Contours of side drag force with different wind speeds.*

At 80.7 m/s wind speed, the force increased to 105 N within 0.13 seconds before to decreasing to 99.5 N after 0.22 seconds and then rose gradually during the wheel acceleration to attain a steady state at 106 N.

At 100 m/s wind speed, the force increased to its peak value of 156 N within 0.12, which is faster and higher than the corresponding force at 80.7 m/s wind speed. The force is seen to undulate slightly whilst still increasing overall to reach 161 N toward the end of the wheel acceleration.

At 120 m/s wind speed, the associated peak value was 203 N within 0.11 seconds, which is the fastest of the three, and has relatively large waves. The steady state value at the end of acceleration was 213 N.

4.3. Lift Force

The downward (negative) lift force of 90 N for all wind speeds is created immediately at wind impact, and occurs just as the wheel starts to rotate. As rotation progresses different force profiles are produced which depend on the wind speed.

Fig. 11 and Fig. 12 show a comparison of the lift forces for different wind speeds and the associated forces profiles respectively. In each case the force increases during the wheel acceleration stage before reaching a steady state.

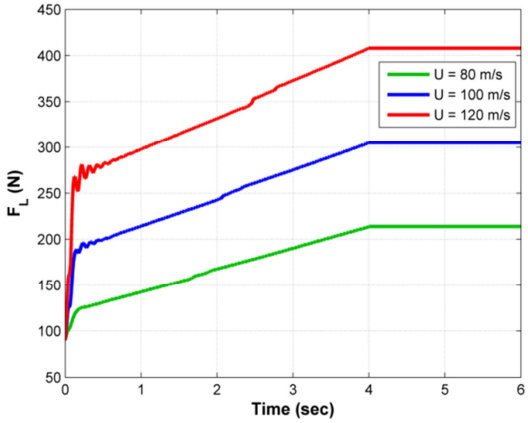

Fig. 11. *A comparison of lift forces vs. time with different wind speeds.*

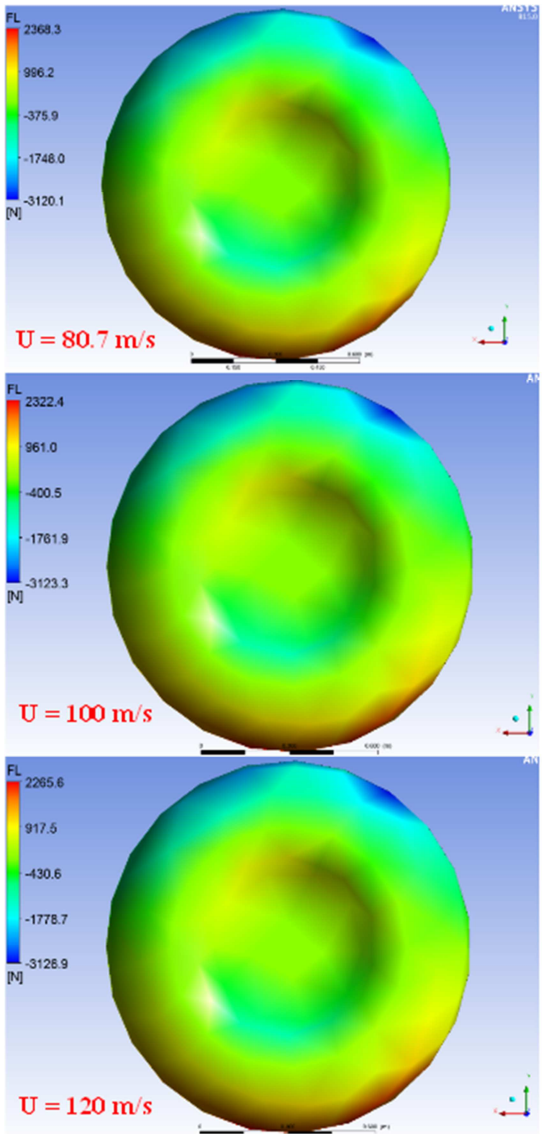

Fig. 12. *Contours of lift force with different wind speeds.*

At 80.7 m/s wind speed, the force increases to 214 N and the maximum vortex value occurs at 2.21 sec. At 100 m/s, and 120 m/s wind speeds, the steady state value of lift forces are 305 N and 408 N respectively, and the maximum vortexes occur at 2.54 sec and 2.83 sec respectively.

4.4. Equivalent Inertial Force During Acceleration

The aircraft approach period offers sufficient time to accelerate the wheel slowly. However, Fig. 13 shows a comparison of equivalent inertia force with different required wheel angular acceleration.

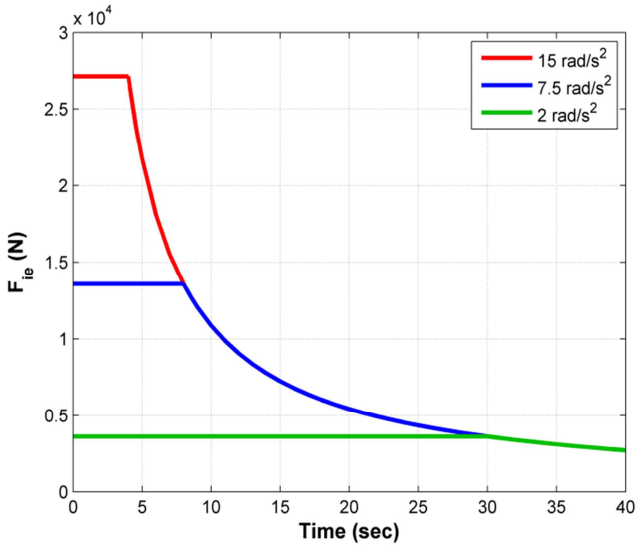

Fig. 13. *Equivalent inertial forces vs. time during different accelerations.*

All the above results are based on an acceleration of 15 rad/s2 which achieves a wheel rotation velocity of 60.5 rad/sec within 4 seconds. Other acceleration values of 7.5 rad/s^2 and 2 rad/s^2 are investigated, which reach the required wheel rotation within 8 and 30 seconds respectively.

The equivalent inertial force to spin the wheel within 4 seconds is 27.13 kN while this changes to 13.6 kN if the time extended to 8 seconds. However, we will use a spin time of 30 seconds which requires a lesser force of 3.6 kN.

4.5. Required Torque

The shaft rolling resistance force is required in order to calculate the total required force and hence to find the required torque.

Fig. 14 shows the rolling resistance forces for the three wind speeds considered. Using the formula in (1), with 0.8 of rim radius, the required torque curves for different wind speeds are presented in Fig. 15. However, in designing the wind turbine, it is necessary to assume a minimum wind speed to be sure the turbine has the capacity to spin the wheel in the worst-case scenario. For our case study, a torque of 1048.7 N.m is sufficient to spin the wheel to 60.5 rad/sec within 30 seconds.

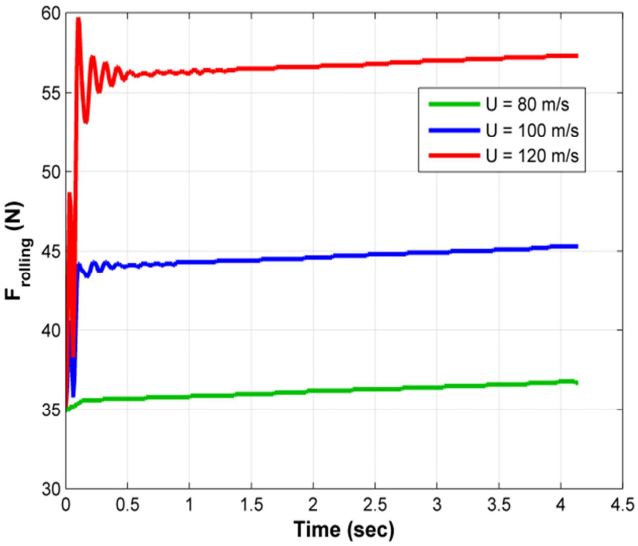

Fig. 14. *Shaft rolling resistance vs. time for different wind speeds.*

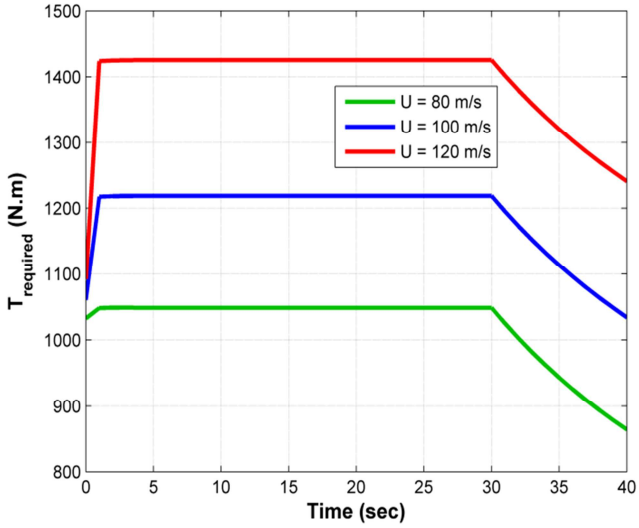

Fig. 15. *Required torque vs. time for different wind speeds.*

5. Conclusion

An isolated wheel has been tested using ANSYS CFX against different wind speeds. The wheel was accelerated from zero to steady state rolling in order to investigate the aerodynamic forces generated during rotation, from this the torque required to spin the wheel was then determined.

We conclude that the lift force depends on the rotation direction. In the aircraft approach condition, the lift force is negative (downwards) and is additive to the load on the wheel. Also, the shape of the tyre has the effect of increasing the drag force in the rotational axis. The required torque calculation procedure is as presented above.

Finally, as a check, it is recommended that a further study should be carried out to include the use of wind turbines in order to test the ability to spin the wheel against various wind speeds. The acceleration time and torque produced should then be considered and compared against the results obtained above.

References

[1] Abbasszadeh, M., T., and Abbasszadeh, M., U.S. Patent Application for a “Apparatus for causing an aircraft wheel to rotate”, Publication No. US20150021435 A1. Washington, DC: U.S. Patent and Trademark Office. 22 Jan 2015.

[2] Sweet, R. M., Gilleran, N., Edelson, J. S., Cox, I. W., Cox, R. T., U.S. Patent Application for a “Integrated electric motor and gear in an aircraft wheel”, Publication No. US8714481 B2. Washington, DC: U.S. Patent and Trademark Office. 6 May 2014.

[3] Karl, W., U.S. Patent Application for a “Free Spinning Wheel for Airplanes”, Publication No. US20140048648 A1. Washington, DC: U.S. Patent and Trademark Office. 20 Feb 2014.

[4] Didey, A., U.S. Patent Application for a “Landing gear drive systems”, Publication No. WO2014023939 A1. Washington, DC: U.S. Patent and Trademark Office. 13 Feb 2014.

[5] Khal, S., and Khal, A., U.S. Patent Application for a “Apparatus for Pre-Rotating Aircraft Tires”, Publication No. US20130112809 A1. Washington, DC: U.S. Patent and Trademark Office. 9 May 2013.

[6] Cassetta, F. G., and Perez, L. C., U.S. Patent Application for a “Passive acceleration device for aircraft wheels”, Publication No. EP1944233 A1. Washington, DC: U.S. Patent and Trademark Office. 16 Jul 2008.

[7] Horvath, V., and Szoke, B., U.S. Patent Application for a “Airplane tire saver by protrusion airfoils”, Publication No. WO2006130944 A1. Washington, DC: U.S. Patent and Trademark Office. 14 Dec 2006.

[8] Robert, A., U.S. Patent Application for a “Self rotating airplane tire”, Publication No. US3773283 A. Washington, DC: U.S. Patent and Trademark Office. 20 Nov 1973.

[9] Beazley, R. H., U.S. Patent Application for a “Aircraft wheel spinner and control”, Publication No. US2414849 A. Washington, DC: U.S. Patent and Trademark Office. 28 Jan 1947.

[10] PADOVAN, JOE, AMIR KAZEMPOUR, and YONG H. KIM. “Aircraft Landing-Induced Tire Spinup.”Journal of Aircraft, Vol. 28, No. 12 (December 1991): pp. 849–854. doi: 10.2514/3.46108.

[11] Saibel, Edward A., and Chenglung Tsai. “Tire Wear by Ablation.” Wear, Vol. 24, No. 2 (May 1973): pp. 161–176. doi: 10.1016/0043-1648(73)90229-9.

[12] Bennett, Michael, Simon M. Christie, Angus Graham, Bryony S. Thomas, Vladimir Vishnyakov, Kevin Morris, Daniel M. Peters, Rhys Jones, and Cathy Ansell. “Composition of Smoke Generated by Landing Aircraft.” Environ. Sci. Technol. Vol. 45, No. 8 (April 15, 2011): pp.3533–3538. doi: 10.1021/es1027585.

[13] T. D. Kothalawala, A. Gatto, and L. Wrobel,”Computational Investigation of the Combined Effects of Yaw, Rotation & Ground Proximity on the Aerodynamics of an Isolated Wheel” International Journal of Mechanical, Aerospace, Industrial, Mechatronic and Manufacturing Engineering, Vol: 7, No: 9, 2013, pp. 1789-1795.

[14] Morelli.A, "Aerodynamic Actions on an Automobile Wheel," Fifth Paper at the First Symposium on Road Vehicle Aerodynamics, City University London, 1969.

[15] Abu Sadek Saifur Rahman, “Computational study on flow around a rotating short cylinder in order to study the effect of rotation on the aerodynamics of a vehicle”, Master Thesis, Texas Tech University, 1996.

[16] Boeing Commercial Airplane Co., “Approach speeds for Boeing airplanes”, 2011. URL: http://www.boeing.com/assets/pdf/commercial/airports/faqs/arcandapproachspeeds.pdf [cited 21 March 2015].

[17] Lufthansa Technik., “Aircraft tires: more than just rubber on steel”, online database, URL: http://www.lufthansa-technik.com/aircraft-tires [cited 11 May 2015].

[18] Goodyear. (2002). Aircraft data tire book. Akron, OH: The Goodyear Tire & Rubber Co., pp. 32-33.

[19] Ochi, Y., and K. Kanai. “Automatic Approach and Landing for Propulsion Controlled Aircraft by H/sub ∞/ Control.” Proceedings of the 1999 IEEE International Conference on Control Applications, Cat. No.99CH36328, 1999, doi: 10.1109/cca.1999.800951.

[20] A. Houari, “Determining the drag coefficient of rotational symmetric objects falling through liquids,” Eur. J. Phys., vol. 33, No. 4, pp. 947–954, May 2012. doi: 10.1088/0143-0807/33/4/947.

[21] J. K. Moore, "Aerodynamics of High Performance Bicycle Wheels", Master thesis, University of Canterbury, 2008.

[22] NASA, “Lift of Rotating Cylinder”, Technical note, URL: https://www.grc.nasa.gov/www/k-12/airplane/cyl.html [Cited 02 Feb. 2016]

[23] Carstensen, S., Mandviwalla, X., Vita, L., and Paulsen, U., “Lift of a Rotating Circular Cylinder in Unsteady Flows”, Journal of Ocean and Wind Energy, Vol. 1, No. 1, 2014, pp. 41–49.

[24] Burns, John A., and Ou, Yuh-Roung., “Effect of Rotation Rate on the Force of a Rotating Cylinder: Simulation and Control” NASA Contractor Report 191442, ICASE Report No. 93-11, 1993, URL: http://ntrs.nasa.gov/search.jsp?R=19930017819 [Cited 17 April 2016]

[25] Zhang, Darui, Andrej Ivanco, and Zoran Filipi. “Model-Based Estimation of Vehicle Aerodynamic Drag and Rolling Resistance.” SAE Int. J. Commer. Veh. 8, no. 2, 2015, pp. 433–439. doi: 10.4271/2015-01-2776.

[26] Bernard J. Hamrock and William J. Anderson., “Rolling-Element Bearings”, NASA Reference Publication 1105, 1983.

[27] Zhang, Xin, Willem Toet, and Jonathan Zerihan. “Ground Effect Aerodynamics of Race Cars.” Appl. Mech. Rev. Vol. 59, No. 1 (2006): pp.33. doi: 10.1115/1.2110263.

[28] Okumura, K., "CFD Simulation by Automatically Generated Tetrahedral and Prismatic Cells for Engine Intake Duct and Coolant Flow in Three Days," SAE Technical Paper 2000-01-0294, 2000, doi: 10.4271/2000-01-0294.

[29] Menter, F. R. “Two-Equation Eddy-Viscosity Turbulence Models for Engineering Applications.” AIAA Journal, Vol. 32, No. 8, 1994, pp. 1598–1605, doi: 10.2514/3.12149.

[30] ANSYS® Academic Research, Release 15.7, Help System, CFX-Pre Guide, ANSYS, Inc.

[31] Menter, Florian R. "Review of the Shear-Stress Transport Turbulence Model Experience from an Industrial Perspective." International Journal of Computational Fluid Dynamics, Vol. 23, No. 4, 2009. pp. 305–316. doi:10.1080/10618560902773387.

[32] Wilcox, D. C., "Turbulence modeling for CFD", 1st ed, La Canada, CA: DCW Industries Inc., 1998.